Development of Electrochemical 6-Well Plates and Its Stability as an Immunosensor

Journal of The Electrochemical Society, 2022 **169** 027506
1945-7111/2022/169(2)/027506/7/$40.00 © 2022 The Electrochemical Society ("ECS"). Published on behalf of ECS by IOP Publishing Limited

Development of Electrochemical 6-Well Plates and Its Stability as an Immunosensor

Feiyun Cui,[1] Zhiru Zhou,[1] Bin Qu,[3] Qin Zhou,[2,z] and H. Susan Zhou[1,z]

[1]*Department of Chemical Engineering, Worcester Polytechnic Institute, Worcester, Massachusetts 01609, United States of America*
[2]*School of Basic Medical Sciences, Harbin Medical University, Harbin Medical University, Harbin 150081, People's Republic of China*
[3]*Biophysics, Center for Integrative Physiology and Molecular Medicine (CIPMM), School of Medicine, Saarland University, 66421 Homburg, Germany*

Developing low-cost and multiplexing electrochemical (EC) devices for bioassay is imperative. Herein, a polymer-based EC device, named EC 6-well plate, was proposed and fabricated using a non-photolithography method. Polyethylene terephthalate glycol (PETG) was used as a substrate and laser-cut polyester (PET) film was used as a mask for patterning the electrodes. The diameter of the working electrode (WE) was 900 μm, and each WE-modifying step only requires 1 μl of reagent. Acrylic mold with wells (60 μl) was bonded to the PETG substrate. Miniaturization of reference electrodes (RE) was discussed. The solid-state Ag/AgCl RE-based three-electrode system, the Au three-electrode system (3E), and Au two-electrode system (2E) were prepared and employed to develop an immunosensor for toxin B detection. Differential pulse voltammetry (DPV) and electrochemical impedance spectroscopy (EIS) were applied to test the stability of the EC immunosensor. The solid-state Ag/AgCl RE-based system showed a standard deviation of open circuit potential (OCP) of 4.6 mV. The 3E system and 2E system showed the standard deviations of OCP of 0.0026 mV and 0.32 mV, respectively. It revealed that the EC 6-well plate with the 3E system is excellent for developing an EC immunosensor.
 [DOI: 10.1149/1945-7111/ac519e]

Manuscript submitted October 16, 2021; revised manuscript received January 13, 2022. Published February 10, 2022. *This paper is part of the JES Focus Issue on Biosensors and Nanoscale Measurements: In Honor of Nongjian Tao and Stuart Lindsay.*

Supplementary material for this article is available online

Electrochemical (EC) biosensors have the advantages of sensitivity, simplicity, and low-cost.[1–4] Meanwhile, they are easy to be miniaturized and batch fabricated.[5–7] Therefore, EC biosensors are very popular in biomedical diagnostics,[4,8–10] environmental monitoring,[11,12] and food safety.[13–15] The development of EC devices that can integrate multiple EC biosensors is an attractive research field. Generally, EC devices can be fabricated by screen printing[16] and photolithography.[17,18] The screen-printing method are widely applied to produce screen printed electrodes.[19,20] However, it is a thick-film fabrication technique which makes the EC biosensor with limited sensitivity. The photolithography method can prepare thin-film electrodes on the silicon or glass.[21,22] It can enhance the sensitivity of EC biosensors. Nevertheless, the fabrication process is complicated and time-consuming. Herein, a novel and user-friendly EC device, named EC 6-well plate, are reported. It was fabricated by a simple, non-screen printing, and non-photolithography method. Polyethylene terephthalate glycol (PETG) is a type of copolymer of polyester (PET) and ethylene glycol.[23,24] It is a transparent amorphous thermoplastic with stable thermomechanical properties and has been employed in biomedical medical devices.[24,25] In addition, it is an excellent polymer substrate for fabricating the chrome/gold (Cr/Au) film electrode.[26] Hence, PETG was used as the substrate to prepare the Cr/Au film electrode and chrome/silver (Cr/Ag) film electrode. Usually, the reported EC devices use silicon or glass as substrates.[27,28] Compared to fragile silicon wafers and glass, PETG has better machining performance and can be a good alternative substrate for fabricating EC devices. PET is the most common thermoplastic polymer in our daily life.[29] Low-cost PET films with various thicknesses are commercially available and they can be easily cut by an affordable laser cutter. Therefore, laser-cut PET film was used as a mask for patterning the electrodes.

For EC biosensors, the stability and robustness of the reference electrodes (RE) often ultimately dictate the stability and sensitivity of EC biosensors. Especially for the electrochemical impedance spectroscopy (EIS) test, the potential at the working electrode (WE) has to remain near redox equilibrium to produce valid impedance results in the system's linear range, RE is necessary to detect and generate stable relevant potentials at the WE.[30] Hence, it is critical to fabricate robust miniaturized RE to facilitate the development of miniaturized EC biosensors. The most preferred RE is the Ag/AgCl electrode based on the half-cell reaction.[31] A fixed chloride concentration is mandatory if a reproducible and stable electrode potential is to be established on the RE. At the same time, it is essential to maintain some solid silver chloride at the surface of the silver electrode to sustain equilibrium. However, a real Ag/AgCl is difficult to be miniaturized on a planar substrate. Solid-state RE can pave the way for miniaturization and cost-effective mass production of reference electrodes. They are mostly used in potentiometric sensors for detecting ions or pH.[32,33] Nevertheless, the influence of solid-state RE on EC biosensors is rarely reported. In this paper, the influence of the solid-state Ag/AgCl RE-based three-electrode system, the Au three-electrode system (3E), and the Au two-electrode system (2E) to DPV and EIS measurements for immunosensors were discussed for the proposed EC 6-well plate.

Experiments

Chemicals and materials.—Potassium ferricyanide ($K_3[Fe(CN)_6]$), potassium ferrocyanide ($K_4[Fe(CN)_6]$), potassium chloride (KCl), potassium nitrate (KNO_3) and hydrochloric acid standard solution (HCl, 1 M) were all purchased from Sigma Aldrich. Cystamine dihydrochloride ($C_4H_{12}N_2S_2$) was purchased from Fluka. 1-(3-dimethylaminopropyl)-3-ethylcarbodiimide hydrochloride (EDC, AR) and N-hydroxysuccin-imide (NHS, AR) were purchased from Thermo Scientific. Ferric chloride ($FeCl_3$, 98%) was purchased from Alfa Aesar. Bovine serum albumin (BSA) was purchased from Sigma-Aldrich. Recombinant TcdB protein and antibodies (sdAbs) against the toxin B of *Clostridium difficile* (TcdB) protein were provided by Professor Feng (University of Maryland Dental School). Highly concentrated graphene oxide dispersion in water (5 g L^{-1}) was purchased from Graphene Supermarket. Polyethylene terephthalate glycol (PETG) sheet (thickness 3 mm), acrylic sheet (thickness 2 mm) and polyethylene terephthalate (polyester, PET) film (thickness 0.5 mm) were purchased from McMaster-Carr.

[z]E-mail: zhouqin@hrbmu.edu.cn; szhou@wpi.edu

Phosphate buffered saline (PBS, 0.1368 M NaCl, 0.0027 M KCl, 0.0081 M Na_2HPO_4, 0.0019 M KH_2PO_4) was filtered through 0.22 μm syringe filters (PES) before use; the water was ultrapure water (18.2 MΩ cm) prepared by Smart-S super pure water machine (Millipore Sigma).

Preparation of electrochemical 6-well plates.—A PETG sheet was used as the substrate for fabricating the electrodes. It was cut into small rectangles of size 40 mm × 28 mm using a band saw (Fig. 1A). The PET mask (Figs. 1B/1J) was designed by AutoCAD software and prepared by VLS-4.60 universal Laser Systems. Double-sided tape was used to bond the PETG sheet and PET mask (Fig. 1C). Cover the RE area with tape and then 10 nm Cr and 100 nm Au films were sputtered onto the PETG sheet using the ATC ORION sputtering system (AJA International, Inc.) (Figs. 1D/1E). Then, the WE and CE area was covered using tapes and the 10 nm Cr and 300 nm Ag films were sputtered on the PETG sheet (Figs. 1F /1G). The PET mask was then carefully removed and the PETG sheet with electrodes was prepared (Figs. 1H/1K).

The acrylic mold with wells was designed by AutoCAD software and prepared by VLS-4.60 universal Laser Systems. Each well which can contain 60 μl of the solution was bonded to the PETG sheet using double-sided tape (Fig. 1I). Finally, The PETG/acrylic device was connected to a printed circuit board (PCB) using copper wires and conductive silver glue (Fig. 1L). The electrochemical wells can be sealed with hydrophilic tape.

Preparation and Characterization of solid-state Ag/AgCl RE.—Both electrochemical (HCl method)[34–36] and chemical methods ($FeCl_3$ method)[37] were applied to prepare the solid-state Ag/AgCl RE. For the electrochemical method, the Ag electrode was used as the WE (Fig. 2A). The potential of the WE was set as 0.001 V, 0.005 V and 0.1 V respectively vs the RE in the 0.1 mol L^{-1} aqueous solutions of HCl. The time was set as 0.1 s, 0.5 s, 1 s, and 3 s. For the chemical method, one drop (3 μl) of 50 mM $FeCl_3$ solution was placed on the Ag electrode for 3 s to chlorinate the Ag layer (Fig. 2A). Graphene oxide (GO) solution was diluted in ultrapure water to reach a concentration of 1 g L^{-1} by ultrasonication for 30 min at 25 °C. 3 μl of the 1 g/L GO solution was placed on the solid-state Ag/AgCl and dried in a drying oven to 40 °C.

The elemental composition and phase structures of the solid-state Ag/AgCl RE were characterized using energy-dispersive X-ray spectroscopy (EDS, Oxford Instruments Nano Analysis) and X-ray Diffraction (XRD, Bruker AXS D8). The morphologies of solid-state Ag/AgCl RE were characterized by scanning electron microscope (SEM, JEOL JSM-7000). After the open circuit potential

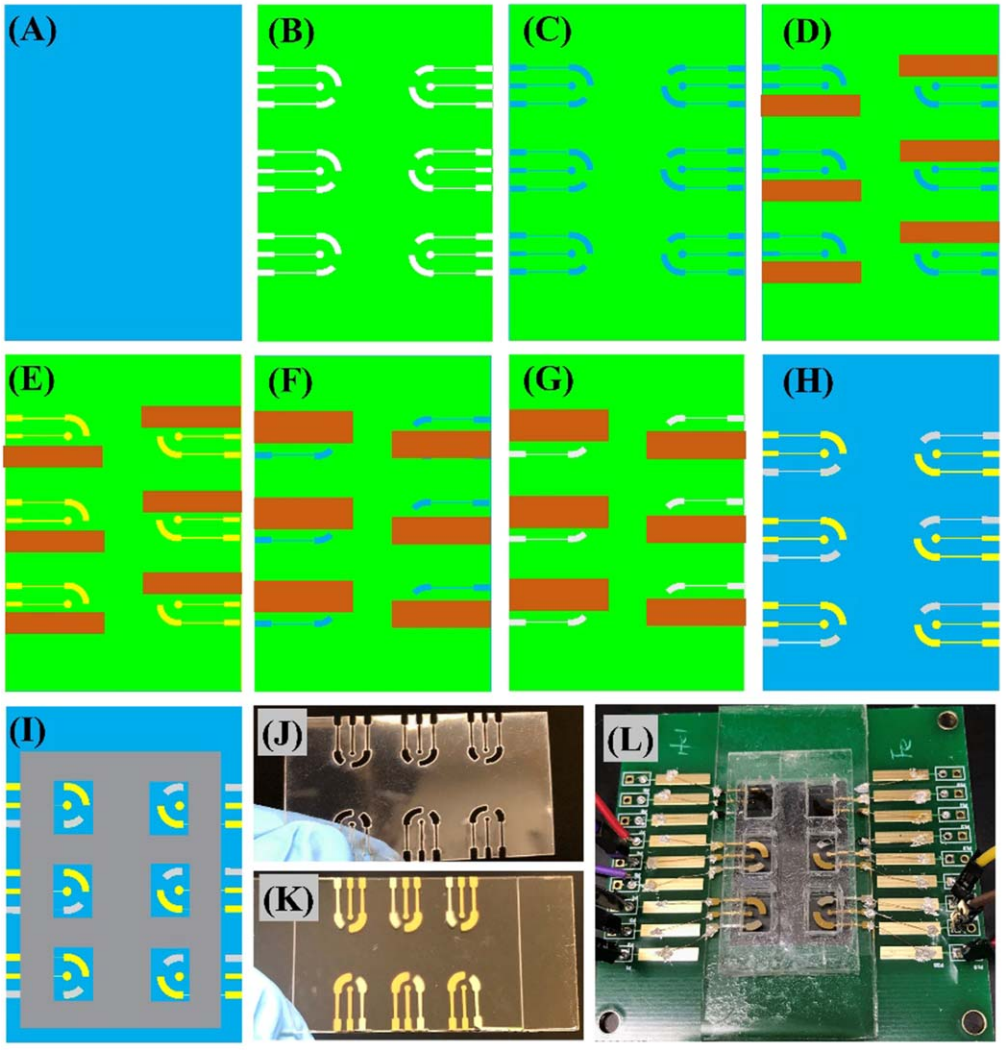

Figure 1. Schematic diagrams to illustrate the preparation of electrochemical 6-well plates. (A) PETG sheet with a size of 40 mm × 28 mm. (B) PET mask. (C) The double-sided tape was used to bond the PETG sheet and PET mask. (D) The tape was used to cover the RE area. (E) 10 nm Cr and 100 nm Au films are sputtered on the PETG sheet. (F) The tape was used to cover the WE and CE area. (G) 10 nm Cr and 300 nm Ag films are sputtered on the PETG sheet. (H) The PET mask was carefully removed and the electrodes are established on the PETG sheet. (I) Double-sided tape was then used to bond the acrylic mold with wells and PETG sheet. (J) Image of PET mask. (K) Image of PETG sheet with 6 groups of electrodes. (L) Image of the prepared electrochemical 6-well plates.

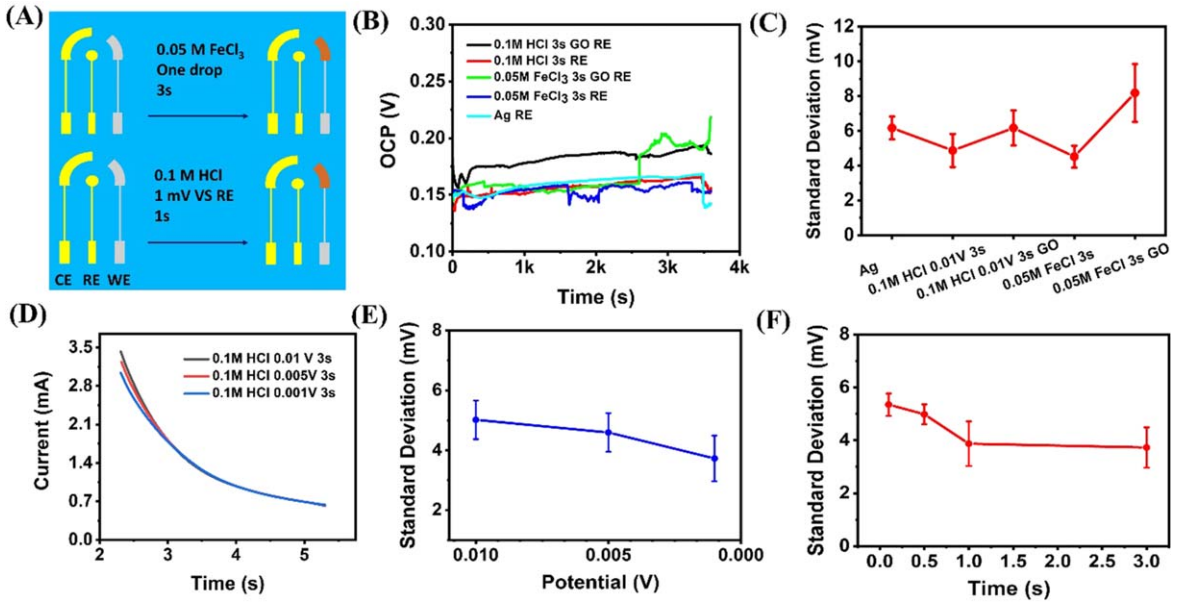

Figure 2. (A) Chemical and electrochemical methods for preparing the solid-state Ag/AgCl RE with final applied parameters. (B) OCP records of Ag, Ag/AgCl ($FeCl_3$ method), Ag/AgCl/GO ($FeCl_3$ method), Ag/AgCl (HCl method), Ag/AgCl/GO (HCl method) as the RE in the presence of 5 mM $K_3[Fe(CN)_6]/K_4[Fe(CN)_6]$ as a redox probe in 0.01 M PBS for 1 h. (C) The standard deviation of OCP was presented (B). (D) Plots of chronoamperometry for preparing the Ag/AgCl (HCl method) with different potentials. (E) Optimization of potential applied to prepare the Ag/AgCl (HCl method, 3 s). (F) Optimization of time duration to prepare the Ag/AgCl (HCl method, 0.001 V). The error bar represents the test results of three groups of electrodes.

(OCP) measurements, the prepared solid-state Ag/AgCl electrode was also examined with SEM and EDS.

Preparation of sensing bio-surface on the WE and detection of TcdB.—The cleaned working electrode (WE) (bare gold) was used as the transducer for the biosensor. Other procedures for the construction of the sensing bio-surface refer to our previous work.[38,39] One drop (1 μl) of 30 mM cystamine dihydrochloride solution was first placed onto the WE overnight and then rinsed with ultrapure water to remove physically adsorbed dithiols. Subsequently, one drop (1 μl) of the sdAb1 solution (1.39 μg ml^{-1}, EDC/NHS-activated) was placed onto the cystamine dihydrochloride self-assembled monolayers (SAMs) modified WE and allowed to react at 4 °C for 2 h. After sufficiently rinsing with ultrapure water, 1 μl of 1% BSA solution was dipped onto the WE for 30 min to block the remaining adsorption reactive sites. Then, the sensing bio-surface on the WE was developed.

1 μl of 1 ng ml^{-1} TcdB solution was placed onto the bio-surface modified WE and incubated at 25 °C for 1 h and thoroughly rinsed with ultrapure water.

Electrochemical test of electrochemical 6-well plates.—All electrochemical measurements were carried out using an Autolab PGSTAT12 electrochemical workstation (Metrohm). Cyclic voltammetry (CV), differential pulse voltammetry (DPV), electrochemical impedance spectroscopy (EIS) and OCP were performed in the presence of 5 mM $K_3[Fe(CN)_6]/K_4$ $[Fe(CN)_6]$ as a redox probe in 0.01 M PBS, 1 M KCl, 0.1 M KCl and 0.1 M KNO_3. The amplitude for the EIS test was 10 mV with 0 V to the OCP, the frequency range was 1–100 kHz. All the experiments were carried out at a Faraday cage.

Results and Discussion

Preparation of electrochemical 6-well plates and solid-state Ag/AgCl RE.—The preparation process of the EC 6-well plate was introduced in Experiments section and the schematic diagram was presented in Figs. 1A–1I. The actual photographs of the PET mask, PETG sheet with 6 groups of electrodes and a finished EC 6-well plate were presented in Figs. 1J–1L. It can be seen that six groups of the three-electrode system were developed on one plate. The diameter of the working electrode is 900 μm (Fig. S1 (available online at stacks.iop.org/JES/169/027506/mmedia)). This novel methodology for fabricating electrodes of electrochemical devices is simple, low-cost, and photolithography-free. For the Au three-electrode system (3E), steps (D) to (G) shown in Fig. 1 can be reduced to one step by sputtering once.

A common strategy for improving the stability of solid-state Ag/AgCl RE is coating a protective layer such as gel or polymer materials.[40,41] However, the coated protective layer can also dissolve relatively rapidly.[42] Recently, GO was demonstrated to be a good protective layer for solid-state Ag/AgCl RE with a potential difference of less than 2 mV for 26 d.[37] Herein, GO coated solid-state Ag/AgCl RE was prepared. They are named as Ag/AgCl/GO ($FeCl_3$ method) and Ag/AgCl/GO (HCl method). For evaluating and comparing the performance of Ag, Ag/AgCl ($FeCl_3$ method), Ag/AgCl/GO ($FeCl_3$ method), Ag/AgCl (HCl method), Ag/AgCl/GO (HCl method) as the RE, the OCP was recorded in the presence of 5 mM $K_3[Fe(CN)_6]/K_4[Fe(CN)_6]$ as a redox probe in 0.01 M PBS for 1 h (Fig. 2B). Standard deviation (SD) of recorded OCP were calculated using Microsoft Excel Worksheet and presented in Fig. 2C. The lower SD value means a smaller drift of potential at WE and a better performance of RE. The results illustrated that both the Ag/AgCl ($FeCl_3$ method) and Ag/AgCl (HCl method) have good performance. The GO coated solid-state Ag/AgCl REs do not show a good performance may be owing to the GO contains different adsorbed ions which can induce significant drifts of the OCP. For these microelectrodes, excessive chlorination would make the RE less conductive and unstable. What's more, a long reaction time can easily cause the Ag/AgCl film to fall off. Hence, precise time control is critical for the performance of the RE and it can prepare reproducible REs which would result in good reproducibility of developed EC biosensors. It is hard to control the time in 1 s or under 1 s using the chemical $FeCl_3$ method. Hence, the electrochemical HCl method was selected for continued work since the reaction time can be precisely controlled.

Optimization of applied potential and reaction time for preparing the solid-state Ag/AgCl RE were conducted. Plots of chronoamperometry for preparing the Ag/AgCl with different potentials are

presented in Fig. 2D. OCP was recorded in the presence of 5 mM $K_3[Fe(CN)_6]/K_4[Fe(CN)_6]$ as a redox probe in 0.01 M PBS for 1 h at different experimental conditions (Fig. S2). The standard deviation of the recorded OCP was shown in Figs. 2E/2F. Characterizations of solid-state Ag/AgCl RE using SEM, EDS and XRD were presented in the Supporting Information section 3 (SI-3).

Influence of different electrolyte on solid-state Ag/AgCl, Au as a RE.—The stability of solid-state Ag/AgCl and drift of OCP can be affected by anions present in the background electrolyte.[43] Exposure of the Ag/AgCl RE to the chloride-containing solution can result in the loss of AgCl from the surface, for example, in the form of $AgCl_n^{(n-1)-}$ complexes.[31] Herein, 0.1 M KCl, 1 M KCl, and 0.1 M KNO_3 containing 5 mM $K_3[Fe(CN)_6]/K_4$ $[Fe(CN)_6]$ were all considered for the electrolyte. Considering that 0.01 M PBS was the most commonly used buffer solution for bioassay, 0.01 M PBS containing 5 mM $K_3[Fe(CN)_6]/K_4$ $[Fe(CN)_6]$ was also included. OCP was recorded using Ag/AgCl (0.1 M HCl, 0.001 V, 1 s) as the RE in the four electrolytes (Fig. 3A). The average of OCP was 148.9 mV (0.01 M PBS), 205.5 mV (1 M KCl), 167.1 mV (0.1 M KCl), and 167.0 mV (0.1 M KNO_3). The standard deviation of OCP was presented in Fig. 3B. They were 4.8 mV, 2.6 mV, 0.41 mV, and 4.4 mV, respectively. These results revealed that 0.1 M KCl was the best choice for the background electrolyte.

OCP of the Au three-electrode system (3E) and Au two-electrode system (2E) were tested in the 0.1 M KCl. Au was used as the RE for both cases. For the same aforementioned reason, 0.01 M PBS is the most commonly used buffer solution for bioassay, the OCP of the Au three-electrode system (3E) and Au two-electrode system (2E) system were also tested in 0.01 M PBS (Fig. 3C). The standard deviations of OCP were presented in Fig. 3D. They were 0.036 mV (0.1 M KCl, 3E), 0.049 mV (0.1 M KCl, 2E), 0.051 mV (0.01 M PBS, 3E), and 0.068 mV (0.01 M PBS, 3E). This data showed that 0.1 M KCl was good for Au as a RE too. For the bare Au WE, the 2E system showed better performance, although it did not display a significant advantage.

Influence of different REs on the stability and repeatability of the immunosensor.—In order to investigate the influence of solid-state Ag/AgCl RE-based three-electrode system, Au three-electrode system (3E), and Au two-electrode system (2E) on an EC immunosensor, the immunosensor was developed by following the steps shown in Fig. S4. Before preparing the sensing surface of the immunosensors, cleaning of WE was needed and the protocols and results were presented in Supporting Information 5 (SI–5).

DPV plots, EIS Nyquist plots, the normalized value of R_{et} (from Nyquist plots) and peak current (PC, from DPV plots) using solid-state Ag/AgCl RE-based three-electrode system were shown in Figs. 4A–4C. Randles equivalent circuit presented in Fig. 4B was used to extract the R_{et}.[44] The direction of the EIS measurement frequency was added in Fig. 4B. Figures 4E, 4H share the same equivalent circuit and direction of the measurement frequency. DPV plots, EIS Nyquist plots, the normalized value of R_{et} and peak current tested by the Au three-electrode system (3E) were shown in Figs. 4D-F. DPV plots, EIS Nyquist plots, the normalized value of R_{et} and peak current tested by the Au two-electrode system (2E) were shown in Figs. 4G–4I. The normalized values of fresh immunosensors and immunosensors stored in 0.01 PBS for 7 d were recorded (Figs. 4C/4F/4I). The SAMs mean self-assembled monolayers of cystamine formed on the WE. Ab means sdAb fixed on SAMs modified WE. BSA means BSA filling nonspecific binding sites, and TcdB means the immunosensor captured the TcdB. Initially, the R_{et} of bare Au electrode in Figs. 4B/4E/4H were 821.6 Ω, 704.8 Ω and 1347 Ω, respectively. After the SAMs of cystamine formation, all three R_{et} were decreased. Small semicircle can be found in the corresponding Nyquist plots. It can be attributed

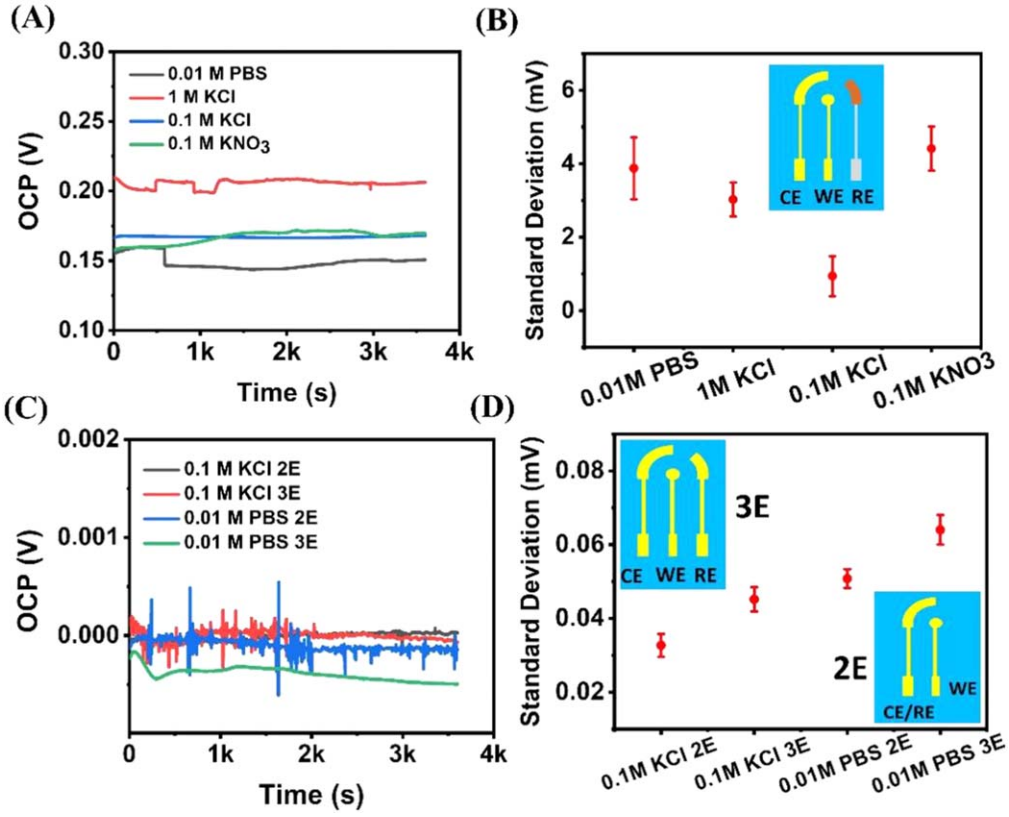

Figure 3. OCP records (A) and their standard deviation (B) of Ag/AgCl (0.1 M HCl, 0.001 V, 1 s) as the RE in the presence of 5 mM $K_3[Fe(CN)_6]/K_4[Fe(CN)_6]$ as a redox probe in 0.01 M PBS, 1 M KCl, 0.1 M KCl and 0.1 M KNO_3 for 1 h. OCP records (C) their standard deviation (D) of Au three-electrode system (3E) and Au two-electrode system (2E) in the presence of 5 mM $K_3[Fe(CN)_6]/K_4[Fe(CN)_6]$ as a redox probe in 0.01 M PBS and 0.1 M KCl. The error bar represents the test results of three groups of electrodes.

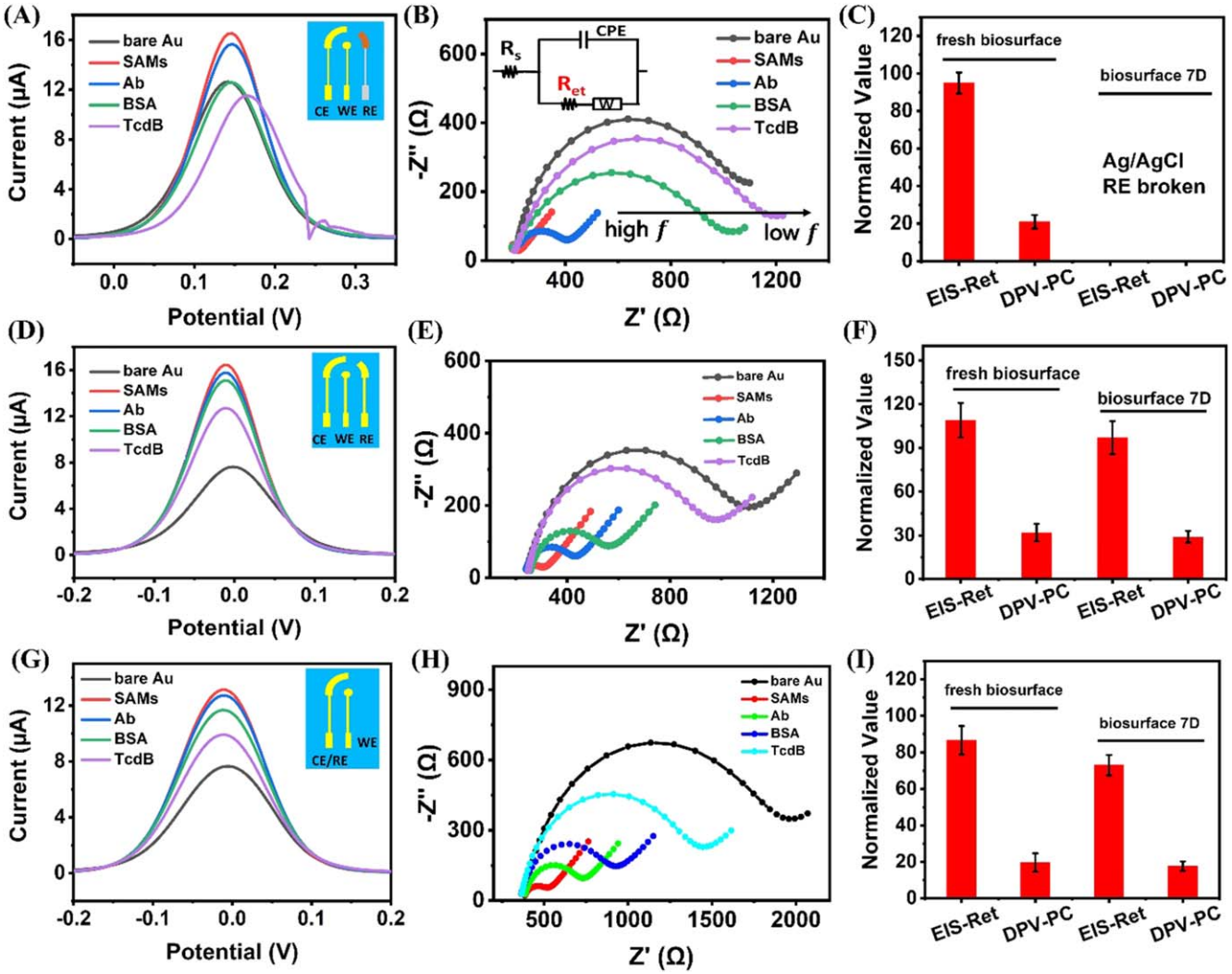

Figure 4. DPV plots (A), EIS Nyquist plots (B) and the normalized value of R_{et} (from Nyquist plots) and peak current (PC, from DPV plots) (C) using Ag/AgCl (0.1 M HCl, 0.001 V, 1 s) as the RE. DPV plots (D), EIS Nyquist plots (E) and normalized value (F) using the Au three-electrode system (3E). DPV plots (G), EIS Nyquist plots (H) and normalized value (I) using Au two-electrode system (2E). All the tests were conducted in the presence of 5 mM $K_3[Fe(CN)_6]/K_4[Fe(CN)_6]$ as a redox probe in 0.1 M KCl. The error bar represents the test results of three groups of electrodes. The Nyquist plots in this figure were adjusted to make the semicircle more obvious and the whole recorded Nyquist plots were presented in figure S6.

to the electrostatic attraction between $-NH^{3+}$ and $[Fe(CN)_6]^{3-/4-}$ which reduce the interfacial charge transfer resistance. This phenomenon has been confirmed in published literature.[45] In this case, all the PC in Figs. 4A/4D/4G were increased. In the following steps including Ab immobilization, BSA filling and TcdB capture, interfacial charge transfer resistances were increased and semicircles of Nyquist plots were extended step by step. Correspondingly, their PC were diminished.

Normalized R_{et} and normalized PC were calculated by the following formulas:

$$\text{normalized value}(R_{et}) = \frac{R_{et(TcdB)} - R_{et(BSA)}}{R_{et(BSA)}} \times 100\% \qquad [1]$$

Where normalized value(R_{et}) is the normalized value of R_{et} of EIS Nyquist plots before and after TcdB was captured by the immunosensor, $R_{et(BSA)}$ is the electron transfer impedance of BSA filled sensing surface and $R_{et\ (TcdB)}$ is the electron transfer impedance after capturing the toxin TcdB.

$$\text{normalized value}(PC) = \frac{PC_{(BSA)} - R_{et(TcdB)}}{R_{et(BSA)}} \times 100\% \qquad [2]$$

Where normalized value(PC) is the normalized value of peak current of DPV plots before and after TcdB was captured by the immunosensor, $PC_{(BSA)}$ is the electron transfer impedance of BSA filled sensing surface and $PC_{(TcdB)}$ is the electron transfer impedance after capturing the toxin TcdB.

Before every EIS test, OCP was recorded in 30 s. The DPV peak position and the OCP related Fig. 4 was listed in Table I. From the bare electrode to the TcdB captured, the DPV peak position drift was 25.18 mV for Ag/AgCl RE-based three-electrode system. The 3E and 2E system almost have no drift. The standard deviation of OCP is about 4.6 mV for Ag/AgCl RE-based three-electrode system, 0.32 mV for the 2E system, and 0.0026 mV for the 3E system. The results demonstrate the high stability and strong robustness of the Au film electrode used as a RE in the EC immunosensor.

Conclusions

In this work, a PETG-based electrochemical 6-well plate was proposed and fabricated using a simple, low-cost, and

Table I. DPV peak position and OCP based on Ag/AgCl RE -based three-electrode system, Au three-electrode system (3E) and Au two-electrode system (2E).

	DPV peak position (mV) (Ag/AgCl)	DPV peak position (mV) (3E)	DPV peak position (mV) (2E)	OCP (mV) (Ag/AgCl)	OCP (mV) (3E)	OCP (mV) (2E)
bare Au	141.75	7.935	12.97	153.5 ± 2.0	−0.3964 ± 0.004	3.382 ± 0.29
SAMs	143.14	12.97	12.97	146.2 ± 0.2	−0.1669 ± 0.003	3.324 ± 0.36
Ab	146.79	12.97	12.97	144.9 ± 2.5	−0.1007 ± 0.001	1.713 ± 0.19
BSA	146.79	12.97	12.97	148.6 ± 16	−0.0382 ± 0.002	2.123 ± 0.27
TcdB	166.93	12.97	12.97	130.8 ± 2.1	−0.4478 ± 0.002	2.725 ± 0.39
BSA 7D	NA	12.97	12.97	NA	−0.0558 ± 0.006	3.160 ± 0.53
TcdB	NA	12.97	12.97	NA	−0.4052 ± 0.002	1.666 ± 0.20

NA: not available.

photolithography-free method. PET film with the designed pattern was used as a mask for preparing the electrodes. The diameter of prepared WE was 900 μm and every step for modifying the WE only need 1 μl of reagent. An in situ chronoamperometry method for the preparation of solid-state Ag/AgCl RE was developed, and the optimal conditions were 0.1 M HCl as the electrolyte and the potential at 0.001 V and time in 1 s. The chlorine content was 5.4%. The solid-state Ag/AgCl RE-based three-electrode system, the Au three-electrode system (3E), and the Au two-electrode system (2E) were used to develop the immunosensor for toxin B of *Clostridium difficile* detection. DPV and EIS were employed to test the stability of the electrochemical immunosensor. The Au three-electrode system (3E) showed just a minor DPV peak position shift and the standard deviation of OCP was about 0.0026 mV. The Au two-electrode system (2E) showed no DPV peak position shift and the standard deviation of OCP was 0.32 mV. The solid-state Ag/AgCl RE-based three-electrode system showed a relatively large DPV peak position shift and the standard deviation of OCP was about 4.6 mV. It is demonstrated that the Au three-electrode system (3E) was superior to the solid-state Ag/AgCl RE-based three-electrode system for developing an immunosensor.

Acknowledgments

This work was supported by the National Science Foundation (CBET-1805514)

ORCID

Feiyun Cui https://orcid.org/0000-0001-5055-1423
Qin Zhou https://orcid.org/0000-0002-6834-354X
H. Susan Zhou https://orcid.org/0000-0002-6659-6965

References

1. J. Liu, W. Lu, L. Zhang, J. Yang, Z.-P. Yao, Y. He, and Y. Li, *Biosens. Bioelectron.*, **193**, 113534 (2021).
2. N. Punnakkal, J. Raveendran, S. Punathil Vasu, B. G. Nair, and T. G. Satheesh Babu, *J. Electrochem. Soc.*, **168**, 047515 (2021).
3. L. Qian, S. Durairaj, S. Prins, and A. Chen, *Biosens. Bioelectron.*, **175**, 112836 (2021).
4. S. Jain, M. Nehra, R. Kumar, N. Dilbaghi, T. Hu, S. Kumar, A. Kaushik, and C.-Z. Li, *Biosens. Bioelectron.*, **179**, 113074 (2021).
5. S. S. Timilsina, P. Jolly, N. Durr, M. Yafia, and D. E. Ingber, *Acc. Chem. Res.*, **54**, 3529 (2021).
6. F. Cui, Z. Zhou, and H. S. Zhou, *J. Electrochem. Soc.*, **167**, 037525 (2020).
7. J. Liu, H. Ji, X. Lv, C. Zeng, H. Li, F. Li, B. Qu, F. Cui, and Q. Zhou, *Microchim. Acta*, **189**, 54 (2022).
8. F. Cui, Z. Zhou, and H. S. Zhou, *Sensors*, **20**, 996 (2020).
9. G. C. M. D. Oliveira, J. H. D. S. Carvalho, L. C. Brazaca, N. C. S. Vieira, and B. C. Janegitz, *Biosens. Bioelectron.*, **152**, 112016 (2020).
10. J. Yang, Y. Hu, and Y. Li, *Biosens. Bioelectron.*, **135**, 224 (2019).
11. X. Cui, J. Han, G. Chen, L. Wang, Z. Luo, C. Chang, J. Zhang, and Q. Fu, *J. Electrochem. Soc.*, **168**, 057508 (2021).
12. P. Rebelo, E. Costa-Rama, I. Seguro, J. G. Pacheco, H. P. A. Nouws, M. N. D. S. Cordeiro, and C. Delerue-Matos, *Biosens. Bioelectron.*, **172**, 112719 (2021).
13. R. T. Paschoalin, N. O. Gomes, G. F. Almeida, S. Bilatto, C. S. Farinas, S. A. S. Machado, L. H. C. Mattoso, O. N. Oliveira, and P. A. Raymundo-Pereira, *Biosens. Bioelectron.*, **199**, 113875 (2022).
14. E. S. McLamore et al., *Biosens. Bioelectron.*, **178**, 113011 (2021).
15. V. S. Manikandan, S. Durairaj, E. Boateng, B. Sidhureddy, and A. Chen, *J. Electrochem. Soc.*, **168**, 107505 (2021).
16. X. Liu, Y. Yao, Y. Ying, and J. Ping, *TrAC, Trends Anal. Chem.*, **115**, 187 (2019).
17. H. A. Abdulbari and E. A. M. Basheer, *ChemBioEng Reviews*, **4**, 92 (2017).
18. A. Mansoorifar, A. Koklu, A. C. Sabuncu, and A. Beskok, *Electrophoresis*, **38**, 1466 (2017).
19. E. P. Randviir, D. A. C. Brownson, J. P. Metters, R. O. Kadara, and C. E. Banks, *Phys. Chem. Chem. Phys.*, **16**, 4598 (2014).
20. A. Hayat and J. L. Marty, *Sensors*, **14**, 10432 (2014).
21. S. Chen, X. Chen, S. Hou, P. Xiong, Y. Xiong, F. Zhang, H. Yu, G. Liu, and Y. Tian, *RSC Adv.*, **6**, 114937 (2016).
22. S. Middya, G. S. Kaminski Schierle, G. G. Malliaras, and V. F. Curto, *Chemical Solution Synthesis for Materials Design and Thin Film Device Applications*, ed. S. Das and S. Dhara (Elsevier, Amsterdam)277 (2021).
23. M. H. Hassan, A. M. Omar, E. Daskalakis, Y. Hou, B. Huang, I. Strashnov, B. D. Grieve, and P. Bártolo, *Polymers*, **12**3045 (2020).
24. Q. Shi, R. Xiao, H. Yang, and D. Lei, *Polymer-Plastics Technology and Materials*, **59**, 835 (2020).
25. I. G. Kim, S. Y. Hong, B. O. Park, H. J. Choi, and J. H. Lee, *Journal of Macromolecular Science, Part B*, **51**, 798 (2012).
26. F. Cui, H. Jafarishad, Z. Zhou, J. Chen, J. Shao, Q. Wen, Y. Liu, and H. S. Zhou, *Biosens. Bioelectron.*, **167**, 112521 (2020).
27. L. Liu, Y. Xu, F. Cui, Y. Xia, L. Chen, X. Mou, and J. Lv, *Biosens. Bioelectron.*, **112**, 86 (2018).
28. R. Wang, Y. Xu, H. Liu, J. Peng, J. Irudayaraj, and F. Cui, *Biomed. Microdevices*, **19**, 34 (2017).
29. C. Bach, X. Dauchy, M.-C. Chagnon, and S. Etienne, *Water Res.*, **46**, 571 (2012).
30. M. Sawhney, E. Azzopardi, S. R. Teixeira, L. Francis, R. Conlan, and S. Gazze, *Electrochem. Commun.*, **105**, 106508 (2019).
31. L. Chen and R. G. Compton, *ACS Sens.*, **4**, 1716 (2019).
32. J. Hu, K. T. Ho, X. U. Zou, W. H. Smyrl, A. Stein, and P. Bühlmann, *Anal. Chem.*, **87**, 2981 (2015).
33. S. Alva, D. Ardiyansyah, D. S. Khaerudini, and R. Suherman, *J. Electrochem. Soc.*, **166**, B598 (2019).
34. P. J. Brewer, A. S. Leach, and R. J. Brown, *Electrochim. Acta*, **161**, 80 (2015).
35. P. J. Brewer, R. J. Leese, and R. J. Brown, *Electrochim. Acta*, **71**, 252 (2012).
36. W. Gao, E. Zdrachek, X. Xie, and E. Bakker, *Angew. Chem. Int. Ed.*, **59**, 2294 (2020).
37. T. Y. Kim, S. A. Hong, and S. Yang, *Sensors*, **15**, 6469 (2015).
38. F. Cui, Z. Zhou, H. Feng, and H. S. Zhou, *ACS Appl. Nano Mater.*, **3**, 357 (2019).
39. Z. Zhu, L. Shi, H. Feng, and H. S. Zhou, *Bioelectrochemistry*, **101**, 153 (2015).
40. P. Lingenfelter, B. Bartoszewicz, J. Migdalski, T. Sokalski, M. M. Bućko, R. Filipek, and A. Lewenstam, *Membranes*, **9**, 161 (2019).
41. G. Schimo, C. D. Grill, J. P. Kollender, and A. W. Hassel, *J. Solid State Electrochem.*, **20**, 2749 (2016).
42. B. J. Polk, A. Stelzenmuller, G. Mijares, W. MacCrehan, and M. Gaitan, *Sensors Actuators B*, **114**, 239 (2006).
43. R. Kalidoss, A. S. Raja, D. Jeyakumar, and N. Prabu, *IEEE Sens. J.*, **18**, 8510 (2018).
44. F. Cui, Y. Xu, R. Wang, H. Liu, L. Chen, Q. Zhang, and X. Mu, *Biosens. Bioelectron.*, **103**, 94 (2018).
45. Z. Mai, X. Zhao, Z. Dai, and X. Zou, *Talanta*, **81**, 167 (2010).